Scientific Research

Synergistic Effect of Fullerene-Capped Gold Nanoparticles on Graphene Electrochemical Supercapacitors

Virginia Yong[*], H. Thomas Hahn

Department of Materials Science and Engineering, University of California, Los Angeles, USA
Email: [*]hyong@ucla.edu

ABSTRACT

We report the synthesis of graphene/fullerene-capped gold nanoparticle nanocomposite film which was used to construct supercapacitor electrodes. The fullerene-based self-assembled monolayers on gold nanoparticles (AuNPs) were attained via the fullerene (C_{60})-gold interaction. The fullerene-capped AuNPs effectively separated the graphene sheets preventing aggregation. A synergistic effect was observed—the specific capacitance of graphene/fullerene-capped AuNP electrode is 197 F/g, which is higher than that of graphene electrode (31 F/g), graphene/AuNP electrode (126 F/g), and graphene/fullerene electrode (118 F/g). The results render a novel route of synthesis and modification of graphene-based materials for the construction of electrochemical energy storage devices.

Keywords: Fullerenes; Gold Nanoparticles; Graphene; Supercapacitors; Energy Storage; Electrochemistry; Self-Assembly; Nanocomposites

1. Introduction

Supercapacitors, also called electrochemical capacitors or ultracapacitors, are considered as a promising candidate for energy storage because of their high power capability, fast charge/discharge rates, long cycle life, and low maintenance cost. The discovery of closed zero-dimensional (0D) buckminsterfullerenes (C_{60}) in 1985 [1] and most recently the experimental isolation of 2D graphene in 2004 [2] by micromechanical cleavage of highly oriented pyrolytic graphite (HOPG) have stimulated much experimental and theoretical research, owing to their unusual structure and extraordinary electronic, transport and optical properties [3]. There has been a tremendous amount of research aimed at developing new carbon-based materials with novel useful applications [4]. Graphene is considered to be an excellent electrode material for supercapacitors due to its high electrical conductivity, high surface area, great flexibility, excellent mechanical properties, and rich chemistry [5]. The surface area of a single graphene sheet is 2630 m^2/g, substantially higher than values derived from Brunauer-Emmett-Teller (BET) surface area measurements of activated carbons used in current electrochemical double layer capacitors [6]. However, aggregation of isolated graphene sheets during drying graphene dispersions leads to a loss of its ultrahigh surface area advantage as a two-dimensional nanomaterial, resulting in low capacitance.

Self-assembled monolayers (SAMs) of alkane thiols on gold nanoparticles (AuNPs) have been the most extensively studied systems due to the well-defined organosulfur adsorption chemistry on Au surfaces [7]. Thiols, thiol esters, or disulfides are well-known to be absorbed onto a gold surface to form a SAM, owing to the strong S-Au bond strength (~180 kJ/mol) [8]. SAMs of fullerenes have attracted increasing interest in many emerging assembly strategies. Previous theoretical and experimental studies have shown that C_{60} can be bound tightly to the gold surface by van der Waals interactions, with a C_{60}-gold binding energy of ~1 eV [9]. The C_{60}-Au bond strength has been reported to be ~200 kJ/mol, [10] which is comparable with the strength of the S-Au bond. They are thus compatible to the thiol-based SAMs on AuNPs which have been extensively studied and exploited in many applications. Recently, AuNPs of 10 nm were used as an efficient spacing material for electrochemically reduced graphene oxide, which greatly increased the capacitance from 4.99 F/g (when no spacers are used) to 174.2 F/g (when gold nanospacers are introduced) [11]. Here, we report a novel route of synthesis and self-assembly processes of fullerene-capped AuNPs which are used as the spacing material of graphene sheets for supercapacitor electrodes.

2. Experiment

Hydrogen tetrachloroaurate trihydrate (HAuCl$_4$·3H$_2$O), dodecylamine (DDA), tetrabutylammonium borohydride

---

(TBAB), and toluene were purchased from Sigma-Aldrich. Didodecyldimethylammonium bromide (DDAB) was purchased from TCI America. Hydrazine monohydrate ($N_2H_4 \cdot H_2O$) was purchased from Fluka. Fullerene derivative [6,6]-phenyl-C61 butyric acid methyl ester (PCBM) was purchased from Nano-C. All reagents and solvents were used without further purification.

AuNPs were synthesized by a seeded growth method [12]. Specifically, DDAB stock solution was first prepared by dissolving 925 mg DDAB in 20 ml toluene. $HAuCl_4 \cdot 3H_2O$ (50 mg) and DDA (450 mg) were added to 12.5 ml of the stock solution and sonicated until dissolved. Gold (III) was then reduced by dropwise addition of 125 mg TBAB in 5 ml of the DDAB stock solution under vigorous stirring. Thus prepared seed (4 nm NPs) solution was aged for 24 hours. The growth solution was prepared by adding 14 ml of the aged seed solution to 100 ml of toluene containing 400 mg $HAuCl_4 \cdot 3H_2O$, 2.00 g DDAB, and 3.7 g DDA. Finally, 262 μl hydrazine dissolved in 40 ml of the stock solution was added dropwise to the growth solution under vigorous stirring. Thus prepared AuNPs have diameters of 5.6 ± 0.6 nm.

A 50 ml sample of the freshly prepared DDA-capped AuNP solution (ca. 7.25 mM) was quenched with 250 ml of methanol to give NP precipitate. The resulting NP precipitate was collected and sonicated in a 3.5 mM toluene solution of PCBM with desired proportions [typically, AuNPs to PCBM in 2:1 (wt/wt)] for 1 hr. The calculated proportions for the formation of a single PCBM monolayer-protected AuNPs in solution and in solid film are 8:1 and 10:3 (AuNPs to PCBM in wt/wt), respectively. A larger amount of PCBM was used owing to the solubility of PCBM in toluene. The as-prepared PCBM-capped AuNPs were then purified by precipitation with a large amount of methanol (90% v/v) followed by several cycles of sonication in toluene, washed with methanol, and re-dispersed in toluene.

Graphene sheets were prepared using the chemical vapor deposition method [13]. The graphene-based nanocomposites (PCBM-capped AuNPs/graphene, AuNPs/graphene, and PCBM/graphene) were synthesized with graphene at a constant fraction of 25 wt%. Typically, 0.15 μg of graphene was mixed with 0.45 μg of PCBM-capped AuNPs (in control experiments, AuNPs or PCBM was used instead of PCBM-capped AuNPs). A 1 μL mixture was deposited on the glassy carbon working electrode surface and dried.

Dynamic light scattering (DLS) was performed on a Beckman Coulter particle size analyzer. X-ray photoelectron spectroscopy (XPS) analyses were conducted using an Omicron ESCA probe operated in vacuum at around 5×10^{-10} torr (1 torr = 133.322 Pa), which was equipped with an EA125 energy analyzer. Photoemission was stimulated by a monochromated Al Kα radiation (1486.6 eV) with an operating power of 300 W. The takeoff angle was set at 45˚. A low-energy electron flood gun was employed for charge neutralization. High resolution TEM (HRTEM) imaging, electron energy loss spectrometry (EELS), and scanning TEM (STEM) studies were carried out using a JEOL 2100 F field emission gun electron microscope operated at 200 kV accelerating voltage. The instrument was equipped with a Gatan slow-scan charge-coupled device (CCD) camera, and Gatan EELS attachments. Cyclic voltammetry (CV) was performed on a Bioanalytical Systems E2-001000 electrochemical workstation. A three-electrode cell was employed for electrochemical measurements, where an Ag/AgCl electrode and a Pt wire were used as the reference and counter electrode, respectively. The cyclic voltammograms were obtained in 0.5 M KCl buffer at room temperature at scan rates of 25, 50, and 100 mV/s.

3. Results and Discussion

AuNPs stabilized by SAMs of fullerene derivative PCBM (**Figure 1(a)**) were prepared as described in the
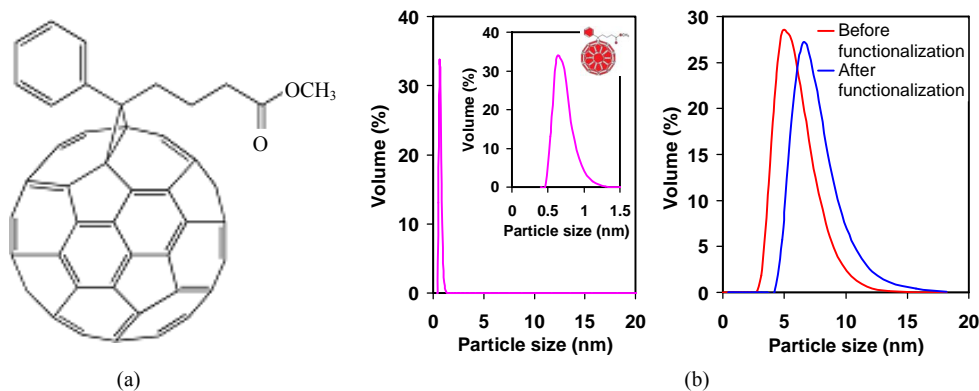

Figure 1. (a) Chemical structure of fullerene derivative PCBM used to form SAMs on AuNPs; (b) DLS showing the particle size distributions of PCBM (0.8 ± 0.1 nm), as-synthesized AuNPs (5.6 ± 0.6 nm), and PCBM-capped AuNPs (7.3 ± 0.7 nm) in toluene, consistent with a single PCBM monolayer-protected AuNPs.

Experiment section. The particle size distributions of PCBM and AuNPs (before and after PCBM functionalization) in toluene were determined using DLS, **Figure 1(b)**. The sizes are ~0.8 nm (PCBM), ~5.6 nm (as-synthesized AuNPs), and ~7.3 nm (PCBM-capped AuNPs), consistent with a single PCBM monolayer-protected AuNPs.

XPS was used to characterize the binding of C_{60} to AuNPs and the oxidation state of gold in the nanoparticles. All spectra were calibrated using the carbon (C1s) peak (284.6 eV) [14]. The high resolution XPS Au 4f spectra of the AuNPs before and after the PCBM functionalization are shown in **Figure 2**. For the AuNPs before the PCBM functionalization, the Au 4f7/2 and 4f5/2 doublet gave rise to peaks positioned at 83.7 eV and 87.4 eV, respectively, consistent with the typical values for Au(0) [15,16]. Bulk Au(0) atoms are known to have Au 4f7/2 binding energy (BE) of 84.0 eV [14] and the negative BE shift could arise from the clean gold surface atoms which caused a shift to a lower BE (of up to −0.4 eV) in comparison with bulk atoms [17]. The observed spin-orbit splitting of 3.7 eV agrees well with the literature value [14]. For the AuNPs after the PCBM functionalization, the Au 4f peaks exhibit a noticeable positive shift of about 0.6 eV yielding binding energies of 84.3 eV and 88.0 eV for Au 4f7/2 and Au 4f5/2, respectively. The binding energy of the Au 4f7/2 for Au(I) has been reported to be ~84.3 to 84.9 eV [15-17]. The observed positive BE shift for AuNPs bound to PCBM indicates that Au atoms were oxidized upon binding to C_{60}, resulting from the charge transfer from Au to C_{60} at the Au/C_{60} interface [18,19].

The PCBM functionalized AuNPs were further investigated using transmission electron microscopy techniques incorporating HRTEM, STEM, and EELS. In EELS, low energy loss spectra provide information about collective electronic as well as single particle/hole excitations associated with transitions between valence and conduction bands. Core loss EELS spectra obtained at higher energy losses can be analyzed to learn about the unoccupied density-of-states via energy-loss near-edge structure (ELNES) and local near neighbor coordination through extended energy-loss fine structure (EXELFS) [20]. HRTEM imaging reveals the presence of extensive periodicity associated with the SAMs of PCBM on AuNPs, **Figure 3(a)**. The AuNPs were found to have a uniform size distribution of ~5.5 nm (consistent with an average diameter of 5.6 nm obtained by DLS measurement in **Figure 1(b)**), and some of which exhibit the characteristic {111} and {200} lattice fringes. An interparticle spacing of ~2 nm was observed, which indicates a single-monolayer of PCBM (~1 nm in length) is on the AuNP surfaces (consistent with the result determined by DLS in **Figure 1(b)**). EELS in STEM line scan mode was employed to examine the PCBM functionalized AuNPs. **Figure 3(b)** shows the atomic-number (Z) contrast STEM image of a discrete AuNP and the corresponding EELS low and core loss spectra at the edge of the AuNP surface. A beam diameter of 5 Å was used to obtain the EELS data, which provides the high spatial resolution capability. The low loss EELS spectrum exhibits "peaks" at ~6 eV and ~25 eV, in which the first peak was assigned to a collective excitation of π elec-
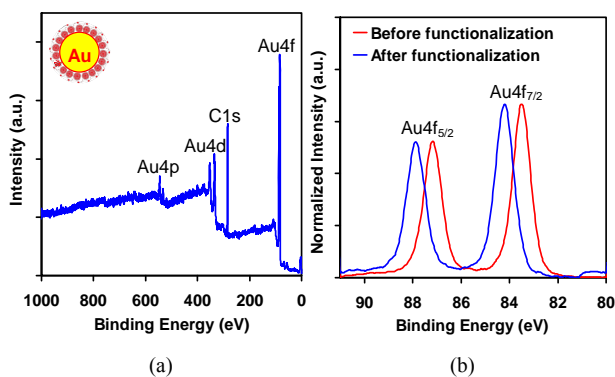

Figure 2. (a) XPS survey spectrum of the PCBM functionalized AuNPs; (b) High resolution XPS Au 4f spectra of AuNPs before and after the PCBM functionalization. Before functionalization, the binding energies of the Au 4f7/2 and 4f5/2 doublet are 83.7 eV and 87.4 eV, respectively. After functionalization, a positive BE shift occurs resulting in binding energies of 84.3 eV and 88.0 eV for Au 4f7/2 and Au 4f5/2, respectively.
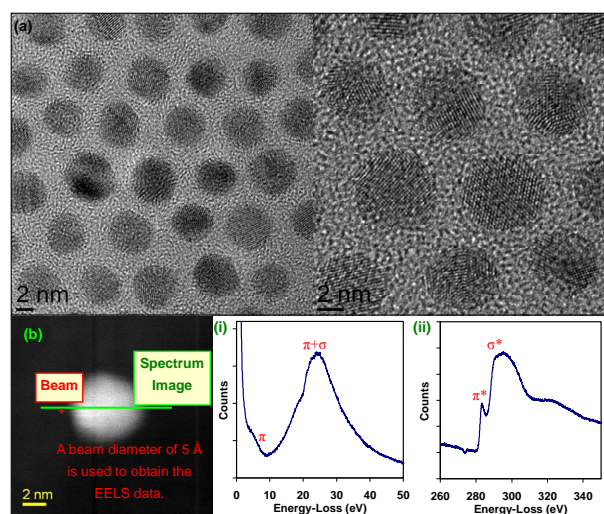

Figure 3. (a) Representative HRTEM micrographs showing the SAMs of PCBM on AuNPs. An interparticle spacing of ~2 nm is observed, which indicates a single-monolayer of PCBM (~1 nm in length) is on the AuNP surfaces; (b) Z-contrast STEM image of a discrete AuNP and the corresponding line scan EELS spectra at the edge of the AuNP surface, which signifies the presence of PCBM on the AuNP surface. EELS showing (i) the low energy loss spectrum with interband π and π + σ plasmons and (ii) the background subtracted 1s core loss spectrum with a π^* transition at ~285 eV and splitting of a σ^* transition centered at ~291 eV.
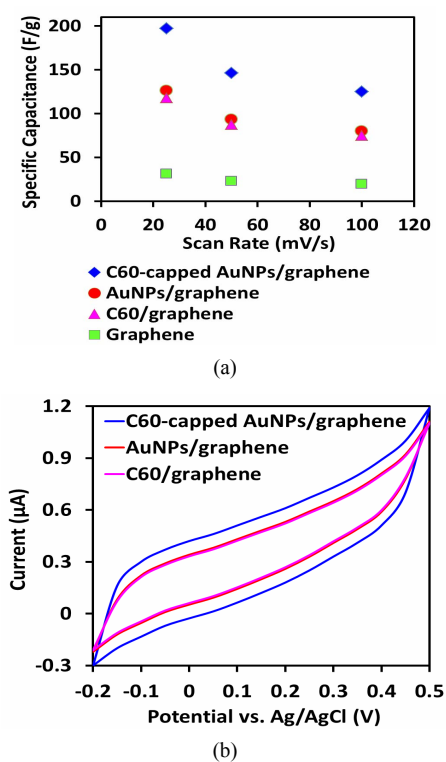
(a)

(b)

Figure 4. Comparison of electrochemical performance of graphene-based nanocomposites. (a) Specific capacitances of fullerene-capped AuNPs/graphene, AuNPs/graphene, fullerenes/graphene, and graphene electrodes in 0.5 M KCl buffer at scan rates of 25, 50, and 100 mV/s; (b) Cyclic voltammograms of fullerene-capped AuNPs/graphene, AuNPs/graphene, and fullerenes/graphene electrodes at a scan rate of 50 mV/s.

trons (*i.e.* an interband π plasmon) and the second broad peak was typically associated with a $\pi + \sigma$ plasmon, **Figure 3(b-i)**. ELNES 1 s features can be utilized as fingerprints of C_{60} at high spatial resolution (<2 nm). Neglecting the core-hole effects, the two common features may be interpreted in terms of π^* and σ^* excitations for the first and second peaks, respectively. The background subtracted 1s core loss spectrum exhibits a π^* transition at ~285 eV and splitting of a σ^* transition centered at ~291 eV, consistent with the fingerprints of C_{60} [21] and hence confirming the presence of PCBM on the AuNP surface, **Figure 3(b-ii)**.

Cyclic voltammetry was used to examine the electrochemical properties, **Figure 4**. **Figure 4(a)** shows the specific capacitance of PCBM-capped AuNPs/graphene nanocomposite film at various scan rates. The specific capacitances of AuNPs/graphene, PCBM/graphene, and graphene films were also determined for comparison. Their cyclic voltammograms are shown in **Figure 4(b)**. The specific capacitance of PCBM-capped AuNPs/graphene electrode is 197 F/g, which is higher than that of graphene electrode (31 F/g), AuNPs/graphene electrode

(126 F/g), and PCBM/graphene electrode (118 F/g). The fullerene-capped AuNPs effectively separated the graphene sheets preventing aggregation—this accounts for the observed synergistic effect.

4. Conclusion

In summary, we have demonstrated that fullerene-capped AuNPs are effective spacing materials of graphene sheets for supercapacitor electrodes. Our fullerene-capped AuNPs/graphene nanocomposite material exhibits excellent electrochemical properties with substantially enhanced capacitance performance when compared with the AuNPs/graphene and fullerenes/graphene electrodes. The capacitance might be further improved by optimizing the size of gold nanoparticles and/or the mass ratio between graphene and fullerene-capped AuNPs. The results render a novel route of synthesis and modification of graphene-based materials for the construction of electrochemical energy storage devices.

5. Acknowledgements

REFERENCES

[1] H. W. Kroto, J. R. Heath, S. C. Obrien, R. F. Curl and R. E. Smalley, "C_{60}: Buckminsterfullerene," *Nature*, Vol. 318, No. 6042, 1985, pp. 162-163. doi:10.1038/318162a0

[2] K. S. Novoselov, A. K. Geim, S. V. Morozov, D. Jiang, Y. Zhang, S. V. Dubonos, I. V. Grigorieva and A. A. Firsov, "Electric Field Effect in Atomically Thin Carbon Films," *Science*, Vol. 306, No. 5696, 2004, pp. 666-669. doi:10.1126/science.1102896

[3] V. Yong and J. M. Tour, "Theoretical Efficiency of Nanostructured Graphene-Based Photovoltaics," *Small*, Vol. 6, No. 2, 2010, pp. 313-318. doi:10.1002/smll.200901364

[4] D. Yu and L. Dai, "Self-Assembled Graphene/Carbon Nanotube Hybrid Filmsfor Supercapacitors," *Journal of Physical Chemistry Letters*, Vol. 1, No. 2, 2010, pp. 467-470. doi:10.1021/jz9003137

[5] L. L. Zhang, R. Zhou and X. S. Zhao, "Graphene-Based Materials as Supercapacitor Electrodes," *Journal of Materials Chemistry*, Vol. 20, No. 29, 2010, pp. 5983-5992. doi:10.1039/c000417k

[6] M. D. Stoller, S. J. Park, Y. W. Zhu, J. H. An and R. S. Ruoff, "Graphene-Based Ultracapacitors," *Nano Letters*, Vol. 8, No. 10, 2008, pp. 3498-3502. doi:10.1021/nl802558y

[7] J. C. Love, L. A. Estroff, J. K. Kriebel, R. G. Nuzzo and G. M. Whitesides, "Self-Assembled Monolayers of Thiolates on Metals as a Form of Nanotechnology," *Chemical Reviews*, Vol. 105, No. 4, 2005, pp. 1103-1169. doi:10.1021/cr0300789

[8] B. Bhushan, "Springer Handbook of Nanotechnology," 3rd Edition, Springer, Berlin, 2010. doi:10.1007/978-3-642-02525-9

[9] H. Park, J. Park, A. K. L. Lim, E. H. Anderson, A. P. Alivisatos and P. L. McEuen, "Nanomechanical Oscillations in a Single-C_{60}Transistor," *Nature*, Vol. 407, No. 6800, 2000, pp. 57-60. doi:10.1038/35024031

[10] G. J. Bubnis, S. M. Cleary and H. R. Mayne, "Self-Assembly and Structural Behavior of a Model Rigid C_{60}-Terminated Thiolate on Au(111)," *Chemical Physics Letters*, Vol. 470, No. 4-6, 2009, pp. 289-294. doi:10.1016/j.cplett.2009.01.071

[11] L. Buglione, A. Bonanni, A. Ambrosi and M. Pumera, "Gold Nanospacers Greatly Enhance the Capacitance of Electrochemically Reduced Graphene," *ChemPlusChem*, Vol. 77, No. 1, 2012, pp. 71-73. doi:10.1002/cplu.201100016

[12] R. Klajn, M. A. Olson, P. J. Wesson, L. Fang, A. Coskun, A. Trabolsi, S. Soh, J. F. Stoddart and B. A. Grzybowski, "Dynamic Hook-and-Eye Nanoparticle Sponges," *Nature Chemistry*, Vol. 1, No. 9, 2009, pp. 733-738. doi:10.1038/nchem.432

[13] V. Yong and H. T. Hahn, "Graphene Growth with Giant Domains Using Chemical Vapor Deposition," *CrystEngComm*, Vol. 13, No. 23, 2011, pp. 6933-6936. doi:10.1039/c1ce05714f

[14] J. F. Moulder, W. F. Stickle, P. E. Sobol and K. D. Bomben, "Handbook of X-Ray Photoelectron Spectroscopy," Physical Electronics Division, Perkin-Elmer Corp., Norwalk, 1995.

[15] J. C. Zhou, X. H. Wang, M. Xue, Z. Xu, T. Hamasaki, Y. Yang, K. Wang and B. Dunn, "Characterization of Gold Nanoparticle Binding to Microtubule Filaments," *Materials Science & Engineering C*, Vol. 30, No. 1, 2010, pp. 20-26. doi:10.1016/j.msec.2009.08.003

[16] M. Brust, M. Walker, D. Bethell, D. J. Schiffrin and R. Whyman, "Synthesis of Thiol-Derivatized Gold Nanoparticles in a 2-Phase Liquid-Liquid System," *Journal of the Chemical Society, Chemical Communications*, No. 7, 1994, pp. 801-802. doi:10.1039/c39940000801

[17] M. C. Bourg, A. Badia and R. B. Lennox, "Gold-Sulfur Bonding in 2D and 3D Self-Assembled Monolayers: XPS Characterization," *Journal of Physical Chemistry B*, Vol. 104, No. 28, 2000, pp. 6562-6567. doi:10.1021/jp9935337

[18] M. Brust, C. J. Kiely, D. Bethell and D. J. Schiffrin, "C_{60} Mediated Aggregation of Gold Nanoparticles," *Journal of the American Chemical Society*, Vol. 120, No. 47, 1998, pp. 12367-12368. doi:10.1021/ja982776u

[19] J. T. Lyon and L. Andrews, "Infrared Spectrum of the Au-C_{60} Complex," *ChemPhysChem*, Vol. 6, No. 2, 2005, pp. 229-232. doi:10.1002/cphc.200400467

[20] V. J. Keast, A. J. Scott, R. Brydson, D. B. Williams and J. Bruley, "Electron Energy-Loss Near-Edge Structure—A Tool for the Investigation of Electronic Structure on the Nanometre Scale," *Journal of Microscopy*, Vol. 203, No. 2, 2001, pp. 135-175. doi:10.1046/j.1365-2818.2001.00898.x

[21] V. P. Dravid, S. Z. Liu and M. M. Kappes, "Transmission Electron Microscopy of Chromatographically Purified Solid State C_{60} and C_{70}," *Chemical Physics Letters*, Vol. 185, No. 1-2, 1991, pp. 75-81. doi:10.1016/0009-2614(91)80143-L